THE ASTROPHYSICAL JOURNAL, 457:764–772, 1996 February 1

THE DISTRIBUTION OF DUST CLOUDS IN THE INTERSTELLAR MEDIUM

ANDREW R. DRING, JAYANT MURTHY, AND R. C. HENRY
Department of Physics and Astronomy, Johns Hopkins University, Baltimore, MD 21218
AND
H. J. WALKER
DRAL, Rutherford Appleton Laboratories, Chilton, Didcot, Oxon, England, UK
Received 1994 July 5; accepted 1995 August 1

ABSTRACT

Murthy, Walker, & Henry (1992) examined 745 O, B, F and G stars on the *IRAS* Skyflux plates in a search for dust clouds that are heated by the stars and found 123 clouds near 106 stars by detection of excess 60 μm emission. We have reanalyzed their sample using the Infrared Sky Survey Atlas (ISSA) data and found 194 clouds near 138 stars. We find a filling factor of (0.02 ± 0.01) for dust of density greater than ~ 3.0 H atoms cm^{-3} to which we are complete. We were able to find a good model fit to the data set with these parameters for the dust clouds: filling factor $= 0.085 \pm 0.03$, scale height $z = 250 \pm 100$ pc, radius power-law exponent $\alpha = -4.26 \pm 0.25$, and density power-law exponent $\beta = -1.15 \pm 0.1$, where the filling factor includes material in the density range 0.01–100 H atoms cm^{-3}; however, there is evidence to suggest that the region probed by these stars is a special environment. We also find significantly lower dust densities near O stars than near B stars.

Subject headings: dust, extinction — ISM: clouds — reflection nebulae

1. INTRODUCTION

The main components of the diffuse emission detected by the *Infrared Astronomical Satellite* (*IRAS*) in the 60 and 100 μm bands are zodiacal light and the cirrus emission of Low et al. (1984) which has it origin in the heating of dust by the interstellar radiation field (ISRF). Some of these dust clouds may lie near enough to a luminous star that heating due to the star is sufficient to let the warmer cirrus cloud be distinguished from cooler background and foreground cirrus clouds. By surveying the volume around luminous stars at known distances from the Sun, a three-dimensional map of the dust distribution can be obtained. Furthermore, if we treat the stars as testing a random sample of the interstellar medium (ISM), we can compare our observations of dust-heated clouds to model cloud distributions in the ISM. This is a powerful probe of the statistical properties of the dust, including its filling factor and the degree to which matter is distributed randomly.

The first attempt at such observations was performed by Van Buren (1989), who looked at a limited region of the sky near the Galactic plane and found a volume-filling factor of 0.2 ± 0.1. More recent attempts have been made by Murthy, Walker, & Henry (1992), who looked at a sample of 745 luminous stars from the Bright Star Catalog (Hoffleit 1982), excluding regions of the galactic disk, and by Gaustad & Van Buren (1993) who looked at all 1808 O and B stars from the Bright Star Catalog. The filling factor found by Gaustad & Van Buren is 0.146 ± 0.024 while Murthy et al. found a filling factor of 0.0008.[1] Murthy et al. reported two dust scale heights of 540 pc and 140 pc for dust associated with more luminous and less luminous stars, respectively. Gaustad & Van Buren did not attempt to measure the dust scale height, but they did suggest that the dust distribution was troughlike near the Sun and correlated with Gould's belt (see Stothers & Frogel 1974 for a description of Gould's belt).

The present work reanalyzes the stellar sample of Murthy et al. using the Infrared Sky Survey Atlas (ISSA), which represents a much improved data set over the Skyflux plates used by Murthy et al. and is comparable to the BigMaps used by Gaustad & Van Buren. We also use a more sophisticated analysis than Murthy et al. to better account for important selection effects. The new search found 194 clouds around 138 stars compared to 123 clouds around 106 stars found by Murthy et al. for the same sample. We find that our data are complete to a density of 3.0 H cm^{-3}, higher than the completeness limit of 0.5 H cm^{-3} for Gaustad & Van Buren since we included clouds that are not centered on the star, and that the filling factor for this material is 0.02 ± 0.01. We also find that the dust density is lower in the vicinity of O stars than it is near stars of other spectral classes.

2. DATA SET

The survey by Murthy et al. used *IRAS* Skyflux plates in the vicinity of 745 stars selected primarily from the Bright Star Catalog (see Murthy et al. for details). They excluded regions within 10° of the Galactic plane and also excluded several regions of known molecular cloud concentrations, such as Orion and Taurus. The spectral type, apparent magnitude, and observed $B-V$ for each star were obtained from the Bright Star Catalog, while the absolute magnitude, temperature, and intrinsic $B-V$ were read from tables in Zombeck (1982), and the $E(B-V)$, spectroscopic distance, and luminosity of the star were calculated from the other quantities.

We incorporated the search criteria of Murthy et al. into fully automated search routines, thus removing the subjectivity of previous searches. This was accomplished by first subtracting the background as described in Murthy et al. and then using a program to identify all the discrete objects on the 60 μm plate in the vicinity of a star. The program identified dis-

[1] This value is a factor of 8 lower than that reported by Murthy et al. because they incorrectly used the radius of the cloud instead of the diameter.

crete objects by locating saddle points in the intensity image. Associated with each saddle point was a two, three, or four-lobed structure, and each lobe was considered to be a discrete object or cloud. Each object was part of a larger object and most objects had several subobjects included inside. When the information governing the object relationships is kept it forms a complete description of the logical structure of the image similar to the structure trees used by Scalo (1990).

Each lobe was considered to be a potential stellar-heated cloud but a single image could contain up to 15,000 objects, most of which were associated with image noise and were only a few pixels in size. In order to eliminate the majority of noise objects we rejected anything smaller than five pixels and objects whose surface brightness was less than 0.1 σ higher than their surroundings. After removing the noise associated objects we were left with 2249 possible clouds. We then computed three parameters: an average temperature parameter rejecting objects whose average temperatures were within 1 σ of the plate average, a change in temperature parameter rejecting objects whose 60 μm excess, as defined by Gaustad & Van Buren, did not increase significantly toward the star in question and a parameter comparing the plate distance to the distance computed by using the 60/100 μm ratio, rejecting objects whose 60/100 μm ratio was too high to be due to the star in question, assuming that the object was at the same distance as the star. After accounting for objects within objects that both satisfy the criteria, we found 194 clouds around 138 stars which are listed in Table 1. Table 2 shows the percentage of clouds rejected by each test during the second cut out of the 2249 clouds allowed by the first cut. Each cloud was inspected visually to ensure the correct operation of the program. The distances of the clouds from the heating star that are listed in Table 1 were determined by setting the predicted 60/100 μm ratio equal to the observed value.

Figure 1 shows the distribution of our target stars on the sky as well as the distribution of stars with dust. Figure 2 shows the distribution of stars, and stars with dust, projected onto the plane of the galaxy, with no evidence for a troughlike feature. The distribution of stars with dust in Figure 2 looks essentially

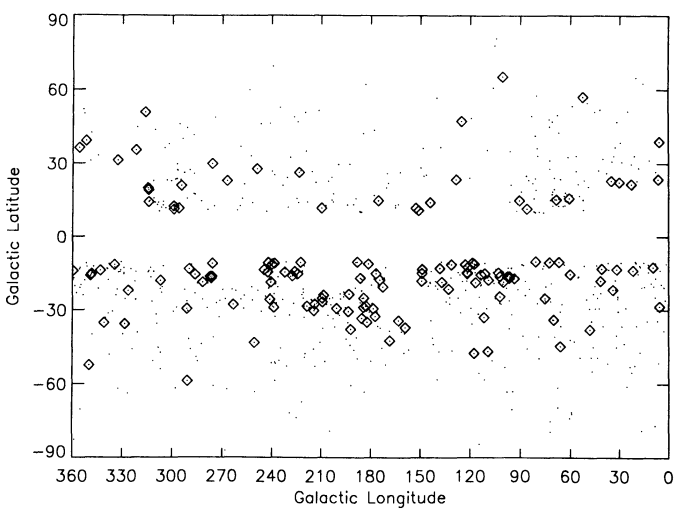

FIG. 1.—The distribution of the stars in our program in Galactic coordinates is shown. Those stars around which we have found dust clouds are plotted as diamonds. Note that we have excluded several regions including the Galactic plane, such as Orion and Taurus (see Murthy et al.).

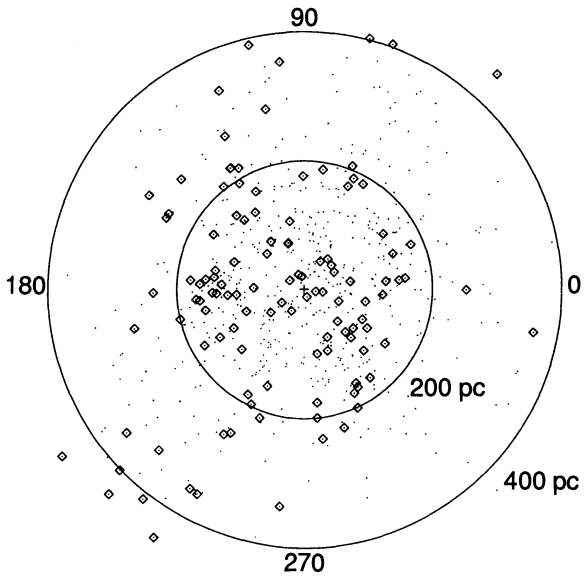

FIG. 2.—The distribution of the stars in our program projected onto the Galactic plane that are within 400 pc of the Sun. Those stars around which we have found dust clouds are plotted as diamonds.

random inside 200 pc, but beyond 200 pc there are considerably more dust clouds between Galactic longitudes 90–270 toward the Galactic anticenter than toward the Galactic center. In particular, there seems to be an excess of clouds in the direction of Galactic longitude 240, the nominal direction of the troughlike feature reported in Gaustad & Van Buren and the direction of the void reported in Frisch & York (1983), although this may be the result of excluding stars from the Galactic plane. Figure 3 shows histograms for the flux, surface brightness, density, and size for both the present sample and the data from Gaustad & Van Buren. The flux, density, and radius were taken from columns (10), (15), and (13), respectively, in Table 2 of Gaustad & Van Buren and the surface brightness was calculated by dividing column (10) by the square of column (13) multiplied by π. Figure 3 shows that there is little difference between the basic results of Gaustad & Van Buren and our work, the only difference is that we have kept a few smaller objects.

3. MODELING

We would like to understand how dust is distributed in the galaxy by comparing the predictions of various dust distribution models with observations. In order to make the comparison we need to understand how dust in the vicinity of a hot star would have appeared in the *IRAS* detectors. Thus, before discussing the dust distribution models, we must construct a detailed model for dust heating and emission in clouds near stars. Consider a volume element $dV = R^2\, d\Omega\, dr$, a distance R away from the illuminating star, subtending a solid angle $d\Omega$, and having radial extent dr. The energy absorbed by dust in this volume at a given wavelength is

$$\Delta E_\lambda = \frac{d\Omega}{4\pi} L_\lambda[\exp(-\tau_\lambda) - \exp(-\tau_\lambda - d\tau_\lambda)](1 - a_\lambda), \quad (1)$$

where L_λ is the luminosity of the star at a given wavelength, a_λ is the albedo at that wavelength, τ_λ is the optical depth from the star to the volume element, and $d\tau_\lambda$ is the optical depth of

TABLE 1

STARS WITH DUST CLOUDS

(1)	HD (2)	Spectral Type (3)	l (4)	b (5)	V (6)	Distance (pc) (7)	r_c (pc) (8)	d_c (pc) (9)	Density (cm^{-3}) (10)	F_{12} ($\times 10^{-5}$ ergs s^{-1} cm^{-2} sr^{-1}) (11)	F_{25} (12)	F_{60} (13)	F_{100} (14)
1.....	358	B8 IV	111.7	−32.8	2.1	29	0.03	0.21	1.68	0.03	0.03	0.06	0.07
2.....	358	B8 IV	111.7	−32.8	2.1	29	0.03	0.15	0.70	0.58	0.15	0.08	0.07
3.....	886	B2 IV	109.4	−46.7	2.8	109	0.11	3.80	8.68	0.04	0.09	0.12	0.29
4.....	886	B2 IV	109.4	−46.7	2.8	109	0.23	3.68	4.02	0.43	0.53	0.51	1.14
5.....	1337	O9 III	117.6	−11.1	6.1	1709	2.75	28.58	1.94	0.19	0.15	0.54	1.74
6.....	1438	B8 V	116.7	−18.7	6.1	180	0.40	0.41	2.03	0.25	0.24	0.68	1.40
7.....	1976	B5 IV	118.7	−10.6	5.6	219	1.29	1.50	12.62	3.26	3.33	18.15	62.21
8.....	3379	B2 IV	117.7	−47.5	5.9	398	0.74	2.61	0.65	0.26	0.37	0.63	1.02
9.....	3901	B2 V	121.4	−12.3	4.8	227	2.02	4.38	3.99	8.23	8.60	45.56	122.42
10.....	4142	B5 V	121.7	−15.0	5.7	229	0.70	1.10	4.55	0.63	0.66	2.84	7.02
11.....	4180	B5 III	121.8	−14.6	4.5	201	1.18	2.89	6.15	4.72	3.08	10.21	32.62
12.....	4881	B9 V	122.9	−11.3	6.2	145	0.35	0.27	12.65	0.54	0.64	3.92	8.40
13.....	10144	B3 V	290.8	−58.8	0.5	24	0.03	1.00	2.06	0.06	0.09	0.09	0.11
14.....	10144	B3 V	290.8	−58.8	0.5	24	0.03	0.75	1.45	0.13	0.09	0.21	0.21
15.....	10205	B8 III	132.9	−21.3	4.9	169	0.62	0.76	0.64	0.70	0.84	1.73	2.92
16.....	10516	B2 V	131.3	−11.3	4.1	146	0.32	5.35	22.72	0.50	0.37	1.25	4.17
17.....	10516	B2 V	131.3	−11.3	4.1	146	0.45	4.03	6.33	1.62	1.34	2.53	6.25
18.....	10516	B2 V	131.3	−11.3	4.1	146	0.13	3.93	3.16	0.01	0.03	0.03	0.08
19.....	12534	B8 V	137.0	−18.6	4.8	85	0.27	0.40	2.86	12.26	3.72	1.58	3.14
20.....	14372	B5 V	138.2	−12.9	6.1	265	0.28	1.41	15.76	0.03	0.05	0.19	0.60
21.....	17543	B6 V	158.9	−37.0	5.2	148	0.22	1.04	8.57	0.14	0.13	0.22	0.65
22.....	18552	B8 V	149.1	−18.1	6.1	174	0.15	0.48	6.47	0.04	0.05	0.08	0.19
23.....	18604	B6 III	168.2	−42.4	4.7	193	0.40	2.83	37.07	0.28	0.38	0.88	3.86
24.....	19356	B8 V	149.0	−14.9	2.1	27	0.02	0.50	47.68	0.04	0.03	0.06	0.16
25.....	19374	B1 V	163.0	−34.2	6.1	592	3.11	8.70	2.74	1.86	4.58	6.10	22.30
26.....	19736	B4 V	148.9	−13.3	6.2	291	0.86	1.83	7.88	0.59	0.55	2.45	7.78
27.....	23793	B3 V	177.2	−32.5	5.1	194	0.68	1.67	3.19	0.83	1.63	5.34	10.51
28.....	24263	B5 V	182.1	−34.9	5.7	176	0.55	1.35	12.29	0.69	1.40	3.12	9.55
29.....	25204	B3 V	178.4	−29.4	3.5	91	0.18	0.77	0.98	0.35	0.67	1.28	1.25
30.....	25340	B5 V	191.9	−37.8	5.3	200	0.55	1.49	14.28	0.41	0.72	1.94	6.60
31.....	25558	B3 V	185.3	−33.3	5.3	203	0.54	1.14	0.57	0.35	0.72	1.37	1.89
32.....	25558	B3 V	185.3	−33.3	5.3	203	0.18	1.74	2.40	0.02	0.06	0.06	0.11
33.....	26356	B5 V	128.4	23.4	5.6	222	0.21	1.27	3.32	0.07	0.03	0.03	0.10
34.....	26571	B9 III	172.4	−20.5	6.1	152	0.45	1.12	29.46	0.82	1.07	3.11	11.31
35.....	26676	B8 V	182.7	−28.4	6.2	157	0.55	0.44	28.64	3.33	5.96	26.85	59.08
36.....	26912	B3 IV	184.2	−28.9	4.3	122	1.41	3.34	27.35	21.54	19.58	90.86	370.99
37.....	28149	B7 V	174.3	−17.7	5.5	163	1.10	0.87	26.83	10.31	16.41	48.07	159.14
38.....	28217	B8 IV	184.2	−25.1	5.9	133	0.23	0.60	28.72	0.20	0.35	0.97	2.95
39.....	28375	B3 V	193.4	−30.6	5.6	232	0.77	1.90	3.40	0.73	1.22	3.84	8.54
40.....	28873	B2 IV	250.4	−43.2	5.1	289	0.95	2.50	0.43	0.49	0.64	1.90	2.95
41.....	29763	B3 V	176.6	−15.1	4.3	135	0.11	3.12	197.09	0.05	0.05	0.32	1.22
42.....	29763	B3 V	176.6	−15.1	4.3	135	0.25	2.33	13.97	0.22	0.59	0.81	2.22
43.....	30211	B5 IV	200.5	−29.3	4.0	112	0.21	0.81	2.02	0.22	0.32	0.42	0.76
44.....	30614	O9 Ia	144.1	14.0	4.3	871	12.83	25.77	0.29	24.70	45.45	243.60	421.42
45.....	30836	B2 III	192.9	−23.5	3.7	297	0.38	7.34	5.68	0.08	0.11	0.24	0.65
46.....	31764	B7 V	186.1	−16.9	6.1	172	0.82	0.78	9.93	2.04	5.17	9.72	28.64
47.....	32343	B2 V	151.0	10.8	5.1	247	1.19	5.35	14.99	3.58	3.93	14.35	47.85
48.....	32612	B2 IV	214.3	−30.2	6.4	529	2.53	5.84	5.07	2.44	1.62	7.54	27.70
49.....	32991	B2 V	181.3	−11.1	5.9	241	1.55	4.67	9.15	6.51	10.16	33.43	96.17
50.....	33328	B2 IV	209.1	−26.7	4.3	200	1.48	4.19	3.23	2.92	4.19	21.44	55.10
51.....	33949	B9 V	213.9	−27.5	4.4	72	0.13	0.38	41.53	0.26	0.22	0.92	2.80
52.....	34085	B8 Ia	209.2	−25.3	0.1	168	0.17	9.72	25.47	0.05	0.05	0.14	0.47
53.....	34085	B8 Ia	209.2	−25.3	0.1	168	0.21	7.71	27.21	0.12	0.15	0.67	1.74
54.....	34085	B8 Ia	209.2	−25.3	0.1	168	0.39	5.80	3.18	0.29	0.39	1.31	2.57
55.....	34085	B8 Ia	209.2	−25.3	0.1	168	0.25	7.82	16.85	0.16	0.11	0.72	1.92
56.....	34085	B8 Ia	209.2	−25.3	0.1	168	0.38	3.34	1.18	5.81	1.92	2.45	2.90
57.....	34085	B8 Ia	209.2	−25.3	0.1	168	0.46	8.36	15.36	0.56	0.75	3.22	9.18
58.....	34233	B5 V	152.7	11.8	6.1	248	1.30	1.79	21.09	2.56	3.69	12.37	51.65
59.....	34447	B3 IV	218.6	−28.4	6.6	404	0.73	1.68	0.72	0.10	0.17	0.33	0.66
60.....	34503	B5 III	208.3	−24.0	3.6	138	0.36	1.77	3.91	0.63	0.60	1.97	3.82
61.....	35532	B2 V	188.0	−10.3	6.2	424	1.34	4.53	7.24	1.27	1.73	6.20	17.28
62.....	37795	B7 IV	238.8	−28.9	2.6	44	0.07	0.12	0.14	0.88	0.50	0.27	0.15
63.....	40494	B2 IV	241.2	−25.6	4.4	205	0.17	3.81	1.81	0.02	0.02	0.02	0.05
64.....	40953	B9 V	291.1	−29.4	5.5	116	0.09	0.48	17.49	0.02	0.01	0.02	0.09
65.....	42933	B3 III	263.3	−27.7	4.8	381	4.07	3.43	0.48	7.46	5.72	29.14	65.23
66.....	43544	B2 V	224.1	−15.1	5.9	416	0.97	6.18	9.85	1.16	0.53	1.06	4.14
67.....	43955	B2 V	227.5	−16.0	5.5	351	0.90	4.75	2.57	0.47	0.36	0.82	2.39
68.....	44743	B1 III	226.1	−14.3	2.0	453	3.74	26.96	3.20	9.52	8.34	24.58	85.75
69.....	44743	B1 II	226.1	−14.3	2.0	453	0.58	14.91	0.48	0.08	0.06	0.10	0.19
70.....	44743	B1 II	226.1	−14.3	2.0	453	0.58	20.30	2.78	0.07	0.09	0.21	0.55

TABLE 1—*Continued*

(1)	HD (2)	Spectral Type (3)	l (4)	b (5)	V (6)	Distance (pc) (7)	r_c (pc) (8)	d_c (pc) (9)	Density (cm^{-3}) (10)	F_{12} (11)	F_{25} (12)	F_{60} (13)	F_{100} (14)
										($\times 10^{-5}$ ergs s^{-1} cm^{-2} sr^{-1})			
71.....	44743	B1 II	226.1	−14.3	2.0	453	0.65	27.47	8.04	0.11	0.10	0.30	1.07
72.....	45871	B4 V	240.5	−18.6	5.7	271	0.67	1.09	0.54	0.28	0.18	0.53	0.98
73.....	46064	B1 V	222.4	−10.5	6.2	633	0.75	9.16	12.03	0.06	0.03	0.27	1.04
74.....	46064	B1 V	222.4	−10.5	6.2	633	0.66	7.79	4.47	0.03	0.04	0.12	0.40
75.....	46328	B0 IV	232.1	−14.5	4.3	424	0.42	13.38	2.61	0.05	0.01	0.04	0.13
76.....	46328	B0 IV	232.1	−14.5	4.3	424	0.39	7.90	1.15	0.03	0.04	0.09	0.17
77.....	47100	B8 III	175.3	14.8	5.2	185	0.58	1.23	5.55	0.84	0.99	2.22	6.02
78.....	50013	B1 IV	242.4	−14.5	4.0	258	1.37	7.74	4.77	2.88	2.34	7.36	23.62
79.....	50013	B1 IV	242.4	−14.5	4.0	258	0.67	8.57	8.07	0.35	0.42	0.99	3.55
80.....	51823	B2 V	238.4	−10.9	6.2	459	0.37	4.04	1.26	0.02	0.02	0.03	0.07
81.....	52089	B2 II	239.8	−11.3	1.5	363	0.79	19.91	2.20	0.18	0.20	0.50	1.42
82.....	52089	B2 II	239.8	−11.3	1.5	363	0.29	17.73	3.02	0.01	0.01	0.05	0.13
83.....	52089	B2 II	239.8	−11.3	1.5	363	0.40	20.52	2.60	0.04	0.05	0.07	0.20
84.....	52089	B2 II	239.8	−11.3	1.5	363	0.29	19.06	6.69	0.01	0.00	0.09	0.24
85.....	52089	B2 II	239.8	−11.3	1.5	363	0.76	29.15	5.58	0.24	0.19	0.27	1.17
86.....	52089	B2 II	239.8	−11.3	1.5	363	0.36	15.27	2.73	0.10	0.06	0.14	0.30
87.....	52089	B2 II	239.8	−11.3	1.5	363	0.61	13.79	1.04	0.14	0.13	0.37	0.71
88.....	52089	B2 II	239.8	−11.3	1.5	363	0.45	19.15	3.11	0.04	0.07	0.15	0.40
89.....	52089	B2 II	239.8	−11.3	1.5	363	1.47	17.30	1.80	1.00	1.36	4.26	10.41
90.....	52089	B2 II	239.8	−11.3	1.5	363	0.43	23.26	10.94	0.37	0.13	0.23	0.77
91.....	52089	B2 II	239.8	−11.3	1.5	363	0.38	25.89	11.07	0.32	0.08	0.11	0.40
92.....	52092	B3 V	244.6	−13.5	5.1	202	0.46	2.86	43.02	0.54	0.70	3.27	11.23
93.....	54031	B3 V	242.1	−10.6	6.3	365	0.36	1.71	1.52	0.04	0.03	0.10	0.20
94.....	58715	B8 V	209.5	11.7	2.9	41	0.05	0.20	1.64	0.49	0.34	0.18	0.19
95.....	66591	B3 V	276.5	−16.9	4.8	183	0.39	1.18	0.47	0.15	0.20	0.47	0.67
96.....	66591	B3 V	276.5	−16.9	4.8	183	0.17	1.92	3.70	0.04	0.02	0.07	0.16
97.....	67536	B2 V	276.1	−16.1	6.3	447	0.46	6.05	7.20	0.05	0.03	0.08	0.31
98.....	68423	B6 V	277.2	−16.2	6.3	242	0.31	1.03	6.17	0.06	0.04	0.16	0.47
99.....	68520	B6 IV	281.6	−18.6	4.3	107	0.25	1.10	23.26	0.28	0.33	1.24	3.95
100.....	74280	B3 V	223.2	26.3	4.3	151	0.71	1.65	0.91	1.34	2.05	2.98	5.77
101.....	74375	B1 III	275.8	−10.9	4.3	446	0.36	14.84	5.52	0.02	0.02	0.05	0.16
102.....	74375	B1 III	275.8	−10.9	4.3	446	1.36	9.47	1.27	0.53	0.85	2.80	5.75
103.....	74375	B1 III	275.8	−10.9	4.3	446	0.51	15.45	8.34	0.03	0.04	0.18	0.60
104.....	74375	B1 III	275.8	−10.9	4.3	446	0.44	15.90	27.31	0.06	0.08	0.34	1.20
105.....	78764	B2 IV	286.2	−15.4	4.7	231	0.28	3.83	2.09	0.06	0.03	0.10	0.24
106.....	78764	B2 IV	286.2	−15.4	4.7	231	0.91	3.27	1.03	1.03	0.71	2.73	5.44
107.....	78764	B2 IV	286.2	−15.4	4.7	231	0.19	4.66	3.41	0.03	0.02	0.02	0.07
108.....	83754	B5 V	248.7	27.8	5.1	181	0.43	0.87	1.26	0.31	0.32	0.64	1.25
109.....	86606	B9 Ib	289.8	−13.1	6.3	3332	6.28	6.02	0.10	0.24	0.15	0.32	0.69
110.....	89353	B9 Ib	266.9	22.9	5.3	1306	2.43	4.75	0.23	5.55	1.49	0.58	1.01
111.....	96314	B8 III	275.8	30.0	5.7	230	0.28	0.68	0.58	0.07	0.07	0.12	0.18
112.....	105382	B6 III	295.9	11.6	4.5	182	1.25	1.61	5.28	7.82	7.29	34.57	81.44
113.....	105435	B2 IV	296.0	11.6	2.6	83	0.67	3.96	10.39	10.19	8.84	46.05	111.52
114.....	105521	B3 IV	294.4	20.9	5.5	215	1.13	2.12	3.62	2.40	2.35	10.28	25.64
115.....	108257	B3 V	299.0	11.2	4.8	176	0.96	2.05	7.75	2.72	3.44	22.58	54.34
116.....	108483	B2 V	299.1	12.5	3.9	169	0.15	5.23	43.68	0.05	0.04	0.19	0.60
117.....	109387	B6 III	125.2	47.3	3.9	134	0.24	1.11	1.04	0.59	0.37	0.28	0.46
118.....	116658	B1 III	316.1	50.8	1.0	113	1.70	4.42	0.25	23.10	63.98	155.12	159.35
119.....	120307	B2 IV	314.4	19.9	3.4	140	0.29	2.43	1.53	0.36	0.55	0.86	1.29
120.....	120315	B3 V	100.7	65.3	1.9	48	0.04	1.27	2.25	0.03	0.02	0.03	0.04
121.....	120315	B3 V	100.7	65.3	1.9	48	0.07	1.03	1.19	0.12	0.06	0.15	0.18
122.....	120324	B2 IV	314.2	19.1	3.0	110	0.15	3.65	7.98	0.10	0.09	0.27	0.59
123.....	120324	B2 IV	314.2	19.1	3.0	110	0.15	3.26	4.40	0.06	0.09	0.21	0.42
124.....	120324	B2 IV	314.2	19.1	3.0	110	0.39	3.48	4.81	0.93	1.22	3.61	7.66
125.....	121263	B2 IV	314.1	14.2	2.5	94	0.16	3.67	14.51	0.21	0.17	0.89	2.00
126.....	121263	B2 IV	314.1	14.2	2.5	94	0.14	4.50	33.98	0.11	0.13	0.67	1.84
127.....	121847	B8 V	321.7	35.5	5.2	119	0.32	0.34	2.28	0.38	0.76	1.64	2.78
128.....	124771	B4 V	306.9	−18.0	5.1	179	1.35	1.67	7.99	6.66	6.22	34.74	99.93
129.....	129433	B9 V	332.7	31.3	5.7	118	0.16	0.24	3.12	0.10	0.13	0.18	0.35
130.....	135742	B8 V	352.0	39.2	2.6	37	0.09	0.37	6.71	0.80	0.95	0.94	1.76
131.....	136849	B9 V	52.4	57.1	5.4	109	0.11	0.27	3.27	0.06	0.03	0.05	0.11
132.....	138764	B6 IV	356.1	36.4	5.2	152	0.43	0.68	1.20	0.42	0.75	0.88	1.71
133.....	140873	B8 III	5.5	39.0	5.4	191	0.71	0.80	0.83	0.77	1.54	2.29	4.08
134.....	149757	O9 V	6.3	23.6	2.6	172	0.15	7.68	1.48	0.02	0.32	0.06	0.10
135.....	156247	B5 V	22.7	21.6	5.9	194	0.37	1.13	6.38	0.22	0.21	0.72	1.83
136.....	157246	B1 Ib	334.6	−11.5	3.3	732	0.93	24.29	8.68	0.05	0.07	0.57	1.79
137.....	157246	B1 Ib	334.6	−11.5	3.3	732	1.08	25.86	4.84	0.12	0.14	0.39	1.32
138.....	157246	B1 Ib	334.6	−11.5	3.3	732	3.20	21.19	1.96	1.05	2.26	8.57	23.06
139.....	157978	B9 V	30.1	22.4	6.1	57	0.05	0.33	18.38	0.02	0.04	0.06	0.14
140.....	159082	B9 V	35.0	22.9	6.4	162	0.24	0.30	7.37	0.12	0.15	0.43	1.01
141.....	165024	B2 Ib	343.3	−13.8	3.7	812	1.00	15.59	1.89	0.06	0.09	0.40	0.87

TABLE 1—*Continued*

(1)	HD (2)	Spectral Type (3)	l (4)	b (5)	V (6)	Distance (pc) (7)	r_c (pc) (8)	d_c (pc) (9)	Density (cm^{-3}) (10)	F_{12} (11)	F_{25} (12)	F_{60} (13)	F_{100} (14)
										($\times 10^{-5}$ ergs s^{-1} cm^{-2} sr^{-1})			
142.....	165024	B2 Ib	343.3	−13.8	3.7	812	0.88	11.57	0.61	0.03	0.06	0.23	0.38
143.....	165024	B2 Ib	343.3	−13.8	3.7	812	5.32	16.39	0.70	3.45	4.47	18.97	43.80
144.....	166841	B9 V	326.3	−22.0	6.3	163	0.22	0.18	1.01	0.10	0.10	0.24	0.34
145.....	169467	B3 IV	348.7	−15.2	3.5	100	0.10	2.47	25.80	0.07	0.06	0.13	0.39
146.....	170523	B3 III	349.2	−15.9	5.1	376	0.63	2.19	0.61	0.45	0.29	0.58	0.84
147.....	172910	B2 V	359.8	−14.1	4.9	260	2.07	3.62	1.56	7.93	10.14	27.86	61.57
148.....	172958	B8 V	60.8	15.7	6.4	194	0.40	0.54	7.80	0.28	0.23	0.89	2.42
149.....	175191	B2 V	9.6	−12.4	2.0	74	0.12	4.52	48.51	0.19	0.30	1.08	3.01
150.....	175191	B2 V	9.6	−12.4	2.0	74	0.13	3.17	12.36	0.18	0.27	0.96	1.86
151.....	175191	B2 V	9.6	−12.4	2.0	74	0.08	5.90	155.84	0.08	0.16	0.32	1.18
152.....	175191	B2 V	9.6	−12.4	2.0	74	0.12	4.39	75.04	0.22	0.57	1.54	4.16
153.....	176318	B7 IV	68.5	15.2	5.9	213	0.27	0.49	1.57	0.08	0.05	0.18	0.32
154.....	181615	B2 V	21.8	−13.8	4.6	152	0.14	3.03	4.71	0.04	0.08	0.14	0.26
155.....	181615	B2 V	21.8	−13.8	4.6	152	0.42	2.59	2.38	17.32	7.00	2.98	4.76
156.....	184915	B0 III	31.8	−13.3	4.9	657	0.72	9.41	0.14	0.04	0.08	0.14	0.16
157.....	184915	B0 III	31.8	−13.3	4.9	657	3.92	17.59	0.40	3.21	4.82	9.78	20.02
158.....	184915	B0 III	31.8	−13.3	4.9	657	0.53	9.81	0.12	0.03	0.04	0.04	0.05
159.....	184915	B0 III	31.8	−13.3	4.9	657	0.86	21.21	2.20	0.09	0.23	0.31	0.76
160.....	187929	F6 Ib	40.9	−13.1	3.9	677	1.86	3.84	3.33	1.69	1.09	1.76	5.74
161.....	188665	B5 V	90.6	14.9	5.1	182	0.21	1.12	8.68	0.07	0.05	0.21	0.53
162.....	188665	B5 V	90.6	14.9	5.1	182	0.19	0.66	0.98	0.04	0.05	0.10	0.14
163.....	189103	B3 IV	5.5	−28.5	4.4	145	0.20	2.37	9.12	0.09	0.12	0.23	0.63
164.....	189775	B5 III	86.0	11.5	6.2	503	1.25	3.30	9.64	7.66	3.56	1.83	6.78
165.....	191639	B1 V	34.0	−21.7	6.5	737	1.05	2.55	0.16	0.11	0.29	0.45	0.49
166.....	191692	B9 III	41.6	−18.1	3.2	59	0.11	0.72	8.93	0.35	0.29	0.45	1.02
167.....	193924	B2 IV	340.9	−35.2	1.9	69	0.10	3.35	4.15	0.10	0.09	0.16	0.33
168.....	193924	B2 IV	340.9	−35.2	1.9	69	0.06	2.15	1.22	0.02	0.03	0.05	0.06
169.....	193924	B2 IV	340.9	−35.2	1.9	69	0.07	4.35	23.09	0.04	0.03	0.13	0.35
170.....	196519	B9 III	328.4	−35.6	5.2	141	0.51	0.71	2.69	0.96	0.63	2.29	5.13
171.....	196740	B5 IV	67.0	−10.4	5.0	177	0.25	0.96	8.20	0.15	0.20	0.65	1.39
172.....	196867	B9 IV	60.3	−15.3	3.8	51	0.09	0.44	44.40	0.20	0.18	0.31	1.09
173.....	199140	B2 III	72.8	−10.5	6.6	1050	4.14	7.07	1.22	0.86	1.13	6.14	16.08
174.....	202904	B2 V	81.0	−10.1	4.4	191	0.20	5.20	16.68	0.05	0.07	0.14	0.45
175.....	202904	B2 V	81.0	−10.1	4.4	191	0.21	2.74	2.57	0.29	0.16	0.21	0.36
176.....	202904	B2 V	81.0	−10.1	4.4	191	0.17	2.97	2.91	0.06	0.02	0.09	0.17
177.....	202904	B2 V	81.0	−10.1	4.4	191	0.22	3.65	4.46	0.14	0.10	0.17	0.37
178.....	202904	B2 V	81.0	−10.1	4.4	191	0.15	3.45	5.31	0.06	0.03	0.08	0.18
179.....	204867	G0 Ib	48.0	−37.9	2.9	568	0.88	1.40	0.34	2.20	0.67	0.26	0.42
180.....	207563	B2 V	75.3	−25.1	6.3	445	1.27	4.36	2.12	0.66	0.99	1.61	4.30
181.....	209288	B5 III	70.0	−34.0	6.4	487	0.51	1.62	0.71	0.03	0.08	0.11	0.19
182.....	209952	B7 IV	350.0	−52.5	1.7	29	0.07	0.16	0.27	1.24	0.60	0.54	0.38
183.....	212571	B1 V	66.0	−44.7	4.7	265	1.51	2.09	0.27	22.79	46.99	29.95	27.92
184.....	212883	B2 V	93.6	−17.0	6.5	503	1.84	2.78	0.48	0.84	1.05	3.78	6.45
185.....	214168	B2 V	96.4	−16.1	5.7	370	1.33	3.93	3.91	1.02	1.21	6.96	16.73
186.....	214680	O9 V	96.7	−17.0	4.9	639	6.72	8.12	0.31	10.69	14.48	68.93	120.39
187.....	214993	B2 III	97.7	−16.2	5.2	583	3.01	7.17	1.79	2.54	2.41	10.70	28.41
188.....	217101	B2 IV	100.1	−18.5	6.2	455	2.83	4.78	2.66	3.83	3.65	15.29	45.11
189.....	217675	B6 III	102.2	−16.1	3.6	112	1.12	1.85	8.18	15.48	13.10	61.74	168.13
190.....	217811	B2 V	103.1	−14.6	6.4	402	1.10	3.11	0.99	0.44	0.73	1.81	3.44
191.....	219927	B8 III	102.3	−24.4	6.3	314	0.51	1.05	3.30	0.15	0.18	0.51	1.18
192.....	222173	B8 V	109.0	−17.6	4.3	80	0.19	0.49	11.99	0.48	0.43	1.24	3.04
193.....	223047	G5 Ib	111.3	−15.0	4.9	1034	1.48	1.27	0.08	0.70	0.25	0.24	0.29
194.....	224559	B4 V	113.6	−15.5	6.5	349	0.98	1.02	0.63	0.54	0.52	1.43	2.50

NOTES.—Col. (7) is the spectroscopic distance to the star from the Sun. Cols. (8) and (9) are respectively, the average radius of the cloud assuming a spherical cloud, and the distance of the cloud from the star, as defined by the average 60/100 μm ratio in the cloud (see text). Col. (10) is the average density in the cloud using the 100 μm flux density. Cols. (11) through (14) are, respectively, the average 12, 25, 60, and 100 μm flux densities of the cloud (ergs s^{-1} cm^{-2} sr^{-1}).

the volume element. In all the clouds considered, $\tau_\lambda \ll 1$, so we assume optically thin nebulae and get

$$\Delta E_\lambda = \frac{d\Omega}{4\pi} L_\lambda \, d\tau_\lambda (1 - a_\lambda) \, . \tag{2}$$

Using a gas-to-dust ratio of $N_H/E(B-V) = 5.8 \times 10^{21}$ atoms cm^{-2} mag^{-1} (Bohlin, Savage, & Drake 1978), which is the value used throughout this work, we have

$$d\tau_\lambda = \frac{1}{1.086} \frac{A_\lambda}{A_V} \left(\frac{N_H R_V}{5.8 \times 10^{21}} \right) = 4.9 \times 10^{-4} \frac{A_\lambda}{A_V} n_H R_V \, dr \, , \tag{3}$$

where A_λ/A_V is the extinction law of Cardelli, Clayton, & Mathis (1989) with $R_V = 3.1$, n_H is the gas density in H cm^{-3}, and dr is measured in parsecs. Combining to get the energy density of absorbed radiation we have

$$dE/dV = 4.12 \times 10^{-60} n_H L_{\rm eff} R_{\rm pc}^{-2} \text{ ergs } s^{-1} \text{ cm}^{-3} \tag{4}$$

where

$$L_{\rm eff} \equiv \int L_\lambda \frac{A_\lambda}{A_V} (1 - a_\lambda) d\lambda \, . \tag{5}$$

Thus we see that what is important is not the bolometric lumi-

TABLE 2

PERCENTAGE OF FIRST CUT CLOUDS REJECTED BY SECOND CUT

Parameter	Value
Temperature above background test	24%
Temperature increases toward star test	18%
Temperature distance smaller than plate distance test.....	80%

TABLE 3

COMPARISON OF LUMINOSITY AND EFFECTIVE LUMINOSITY

Spectral Type (1)	L ($L_\odot$) (2)	$L_{\rm eff}$ ($L_\odot$) (3)	T (R = 1 pc) (K) (4)	$T_{\rm eff}$ (R = 1 pc) (K) (5)
B9 V	95	79	15.9	15.4
B5 V	830	970	22.8	23.3
B2 V	5700	12900	31.4	36.0
O8 V.....	170000	189000	55.3	56.3

NOTES.—Col. (2) is the bolometric luminosity for the star used by Gaustad & Van Buren and col. (3) is the computed effective luminosity for the same star used in this work. The effective luminosity is essentially normalizing the luminosity to give temperature and is thus larger than the bolometric luminosity for hotter stars and less than the bolometric luminosity for cooler stars. Cols. (4) and (5) are the dust grain temperatures computed from cols. (2) and (3), respectively.

nosity but an effective luminosity which takes account of the optical properties of the dust. Table 3 compares the effective luminosity with the bolometric luminosity for several spectral types. The effective luminosities in this work were calculated using Kurucz (1979) model atmospheres for the stars and grain albedos from Draine & Lee (1984). Assuming that all the energy absorbed is reradiated isotropically in the infrared, the emissivity is just $dE/4\pi\, dV$. Using dust properties from Draine & Lee, we equate grain heating to cooling and integrate over grain sizes to obtain the temperature

$$T = 1.54 \times 10^5 (dE/dV n_{\rm H})^{1/6} = 42.0 L_{\rm eff_{38}}^{1/6} R_{\rm pc}^{-1/3}\ {\rm K}\ . \quad (6)$$

This is essentially the same as equation (1) of Gaustad & Van Buren except that it correctly accounts for the hardness of the radiation by using the effective luminosity. Table 3 shows the difference between equation (7) and that of Gaustad & Van Buren for R = 1 pc, which is largest for early B stars. Finally, with an estimate of the geometry, one can generate an image in any desired *IRAS* band by convolving the dust emission profile with the instrument response function.

To understand how dust is distributed in the galaxy, we compute the number of nebulae we expect to see for each star for a given cloud distribution model and compare with our observations. To compute the expected number of nebulae for each star we consider a large volume around the star, s^3, as shown in Figure 4. If we use spherical clouds of uniform

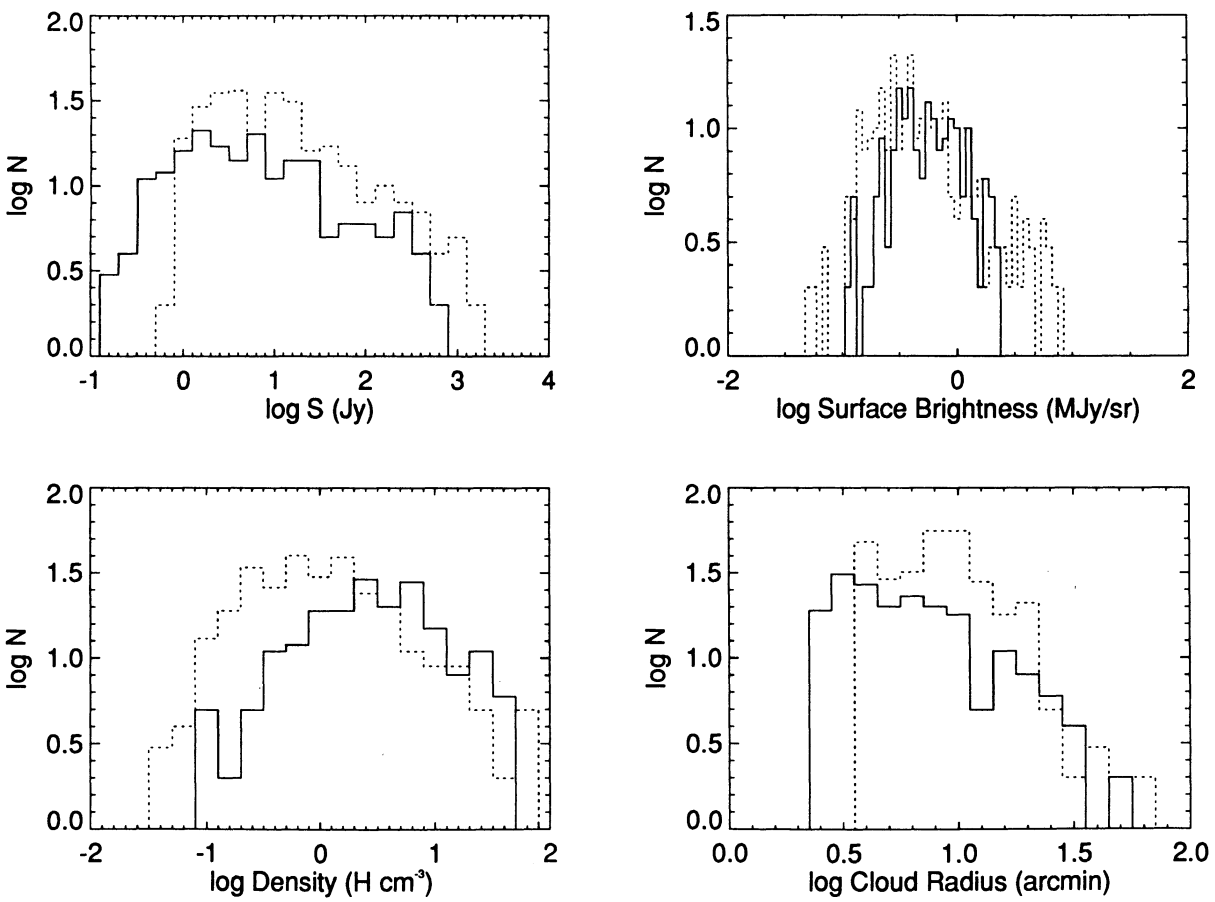

FIG. 3.—Histogram plots for the flux (*upper left*), surface brightness (*upper right*), density (*lower left*), and size distributions (*lower right*) in units of Jy, MJy sr^{-1}, H cm^{-3}, and arcmin, respectively. The dotted lines represent the data from Gaustad & Van Buren and the solid lines represent the Murthy et al. data. The flux and surface brightness plots are for the 60 μm band.

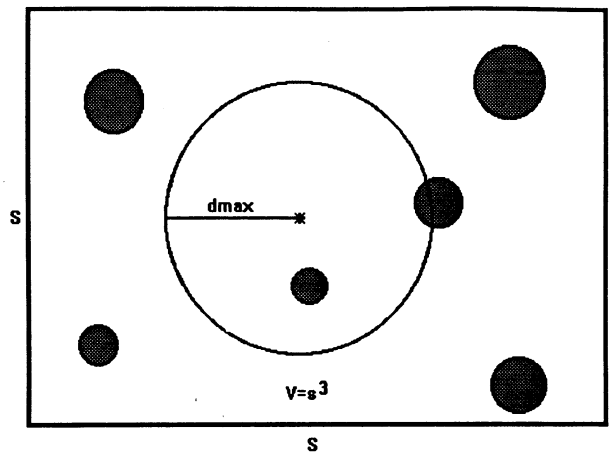

FIG. 4.—Method used to compute the expected number of clouds for each star. When the effective luminosity, cloud radius, density, resolution, and sensitivity of *IRAS* are all given, it is straightforward, given the dust emission model in the text, to compute the maximum distance out to which the cloud can be seen. The probability that the cloud will be detected is $4\pi/3(d\ \max/s)^3$ and integrating over all clouds gives the expected number of observed clouds for each star.

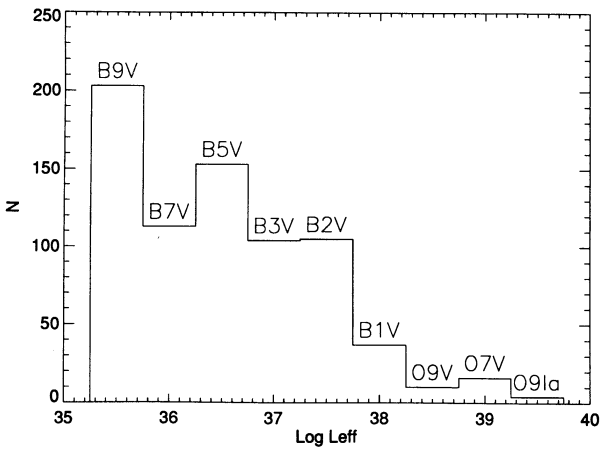

FIG. 5.—A histogram of the number of stars as a function of their effective luminosity for the Murthy et al. sample with a bin size of 0.5 ergs s^{-1} mag^{-1}. For reference a typical spectral type is printed over each bin.

density and distribute them randomly throughout the volume, then we can compute the probability for each cloud that it will be close enough to the star to be observed. The value of s will drop out of the calculation since we will fill the volume to a given filling factor. For a star with a given $L_{\rm eff}$ and a cloud with a given radius and density, we can compute the maximum distance ($d_{\rm max}$) out to which the cloud may be seen given the spatial resolution and sensitivity of *IRAS*. The probability that the cloud is observed is just $(4\pi/3)(d_{\rm max}/s)^3$. We can then integrate over all clouds to compute the expected number of nebulae for each star, with a lower size cutoff for unresolved clouds. The predicted number of observed nebulae for any subgroup of stars can be directly compared with the observations using a χ^2 analysis. The cloud distribution model uses a power-law distribution for the cloud radius with exponent α, a power-law distribution for the dust density in the cloud with exponent β, and a single component exponential scale height z. The volume-filling factor is just the total volume of clouds divided by the total volume of our sample space.

4. RESULTS

Since the radiation fields differ dramatically for different spectral types, it is important to separate the sample of Murthy et al. into subgroups based on their effective luminosity. Figure 5 shows a histogram of the sample binned according to $L_{\rm eff}$, with representative spectral types for each bin. Figure 6 shows a histogram of the number of nebulae found in each bin with an estimate of the uncertainty, assumed to be the square root of N, shown by the error bars. We allowed the volume-filling factor, scale height, and power-law exponents for size and density of the nebulae to vary freely and attempted to find the parameter values which could best reproduce our observations. The best fit to the data using all bins is shown as crosses in Figure 6 and uses the parameters: filling factor $= 0.085 \pm 0.003$, $z = 250 \pm 100$ pc, the radius power-law exponent $\alpha = -4.26 \pm 0.25$, and the density power-law exponent $\beta = -1.15 \pm 0.1$, which produced a reduced $\chi^2_5 = 3.1$.

The filling factor of 0.085 ± 0.03 is considerably lower than the filling factor of 0.25 of McKee & Ostriker (1977) for the warm ionized medium. The power-law index for the size distribution $\alpha = -4.26 \pm 0.25$ is consistent with the value $\alpha = -4.0$ in McKee & Ostriker but inconsistent with the value $\alpha = -2.6$ of Knude (1981) or with the value of $\alpha = -2.3$ of Sanders, Scoville, & Solomon (1985) although the latter looked at dense CO clouds which may not be comparable to the clouds in the Murthy et al. survey. Our scale heights are larger than the estimate of Nandy et al. (1978) of $z = 110$ pc for the agent of extinction at 2200 Å, but the scale height is not well determined in this survey as can be seen by the large uncertainty in the scale height. Finally, our value of $\beta = -1.15 \pm 0.1$ is inconsistent with the value $\beta = -0.5$ taken from Figure 5 in Knude (1979), but agrees well with the value of $\beta = -1.25$ of Gaustad & Van Buren.

The low value of α found by Knude and by Sanders et al. is most likely a selection effect, which is present in this work also as can be seen by the log N-log R relationship from Figure 3. The slope of the plot is $\alpha = -1.1$ for our sample, but many small clouds must go unresolved as can be seen by Figure 7, since those stars which illuminate the greatest region of space

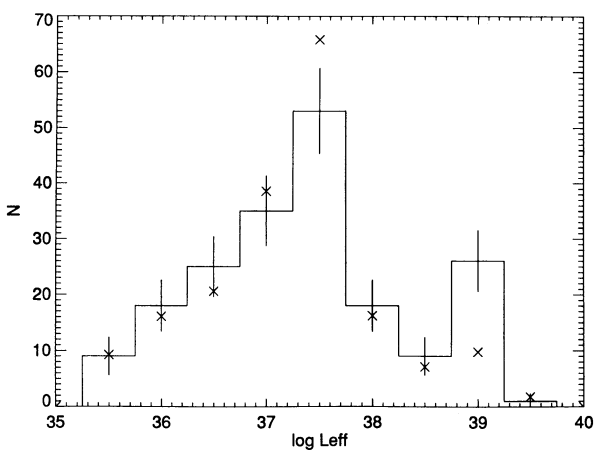

FIG. 6.—A histogram of the number of nebulae as a function of the effective luminosity of the associated stars with a bin size of 0.5 ergs s^{-1} mag^{-1}. The crosses represent the lower reduced χ^2 model for all the stars with the parameters: filling factor = 0.085, $z = 250$ pc, $\alpha = -4.26$, and $\beta = -1.15$ and a reduced χ^2 of $\chi^2_5 = 3.1$.

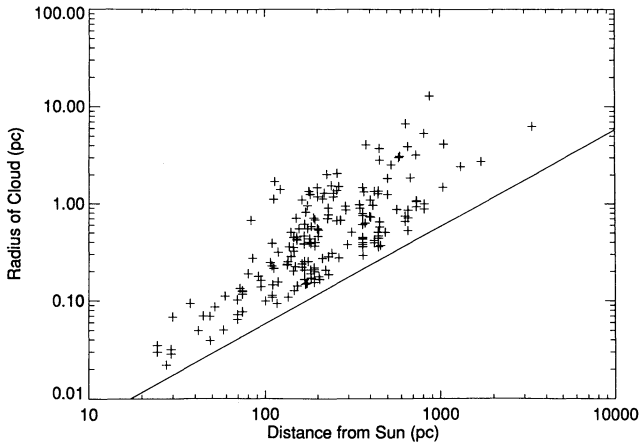

FIG. 7.—A plot of the radius of our cloud vs. the distance from the Sun. The lower envelope of these radii is due to the finite spatial resolution of the instrument, shown by the solid line.

are also the farthest away, it is not possible to see the smallest clouds near them.

The method used to calculate the filling factor in Murthy et al. is particularly sensitive to the estimate of the total volume probed. In Murthy et al. this volume was estimated by determining the point at which the ISRF became equal to the radiation field of the star in question. A second way to estimate this volume is to use equation (5) for the temperature as a function of distance from the star. Since the temperature depends on the distance to the $\frac{1}{3}$ power, the total volume probed goes as T^6, but we can make a more accurate estimate of the average interstellar temperature, or more appropriately the effective limiting temperature for observing a cloud. Figure 8 shows a histogram of the number of clouds as a function of their 60/100 μm ratio for our sample. Although the result is model-dependent, we have calculated temperatures using an emissivity proportional to ν^2 and placed the calculated temperatures across the top of the plot. The distribution falls off rapidly below 24 K. Using the value of 24 ± 1.5 K for the minimum temperature needed to observe a cloud, the total volume probed is $6.4 \pm 2.4 \times 10^5$ pc^3 for all stars and $5.5 \pm 2.0 \times 10^4$ pc^3 for just the B stars. Using a cloud volume of 1.4×10^4 pc^3 for all stars and a cloud volume of 2.5×10^3 pc^3 for B stars we obtain filling factors of (0.02 ± 0.01) and (0.045 ± 0.02), respectively, for dust densities down to our completeness limit of ~ 3.0 H cm^{-3}. The filling factor for all stars is more than a factor of 2 lower because the O stars provide over 90% of the total volume probed, independent of the method used to determine the total volume, and there are few clouds associated with the O stars. To compare this estimate with our model we need to remember that the filling factor of 0.085 in our model is for dust with densities in the range 0.01–100 H cm^{-3}. The fraction of dust greater than ~ 3.0 H cm^{-3} for our power law of $\beta = -1.15$ is 0.23 yielding a filling factor of 0.019 for our model in the appropriate density range.

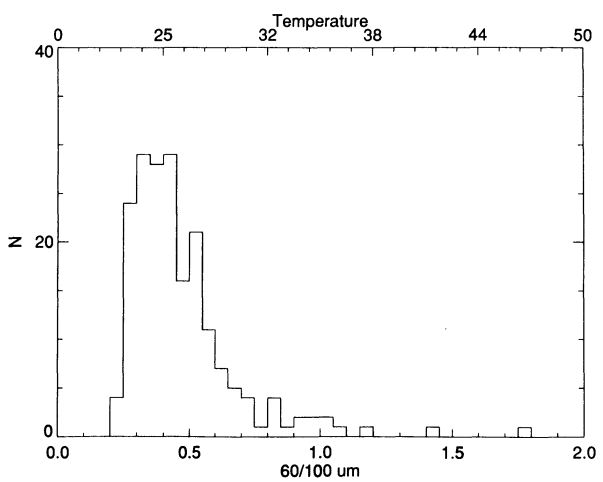

FIG. 8.—A histogram of the number of clouds with a given 60/100 μm ratio. The top of the plot gives the equivalent temperature calculated using an emissivity proportional to ν^2. The distribution falls off rapidly below 24 K.

While it is convenient to quote filling factors as a single number, it is important to remember that they are a function of density. Figure 9 shows the upper limit of the filling factor as a function of density that was calculated on a pixel by pixel basis. The upper limit was calculated by assuming that all the emission in a given pixel was thermal emission from hot dust near the star. The space density was obtained by dividing the intersection of our line of sight with the sphere of influence of the star, into the column density. It should be remembered that even after the smooth background subtraction, there is still dust along the line of sight that is not associated with the star, and that the true filling factor for this density range will be lower. Figure 9 shows again the difference between O and B stars. At 1.0 H cm^3 the upper limit on the filling factor is a factor of 10 lower for O stars and is even lower at higher densities, emphasizing that the environment near O stars is filled with very low density gas.

The filling factors quoted in this work are much lower than the filling factors found by other means, for example, Bohlin et al. (1978) find an average gas density of ~ 1.0 H cm^{-3} implying a much higher filling factor. The reason our filling factors are so low is that we are looking toward a special environment. This is shown in Figure 10 which plots the upper limit of the gas density as a function of distance from the star. Within 3 parsecs of the star the upper limit is lower than the pervading

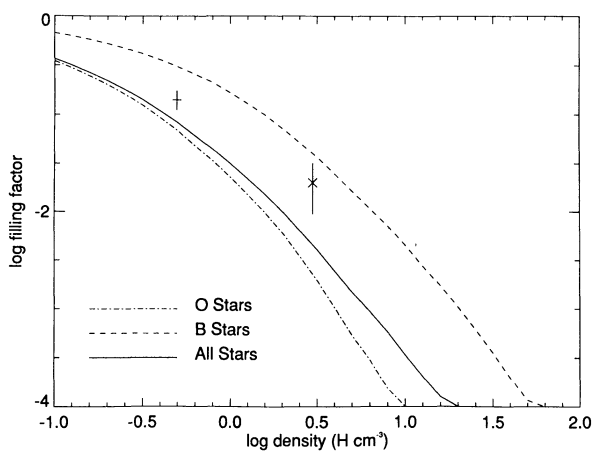

FIG. 9.—A plot of the upper limit of the filling factor for densities greater than or equal to the abscissa. The upper limit was calculated on a pixel by pixel basis assuming all of the 60 μm emission was dust thermally heated by the star and the volume for each pixel was calculated using the intersection of our line of sight with the sphere of influence of the star. Also plotted are curves for the O and B stars alone as well as the filling factors quoted by Gaustad & Van Buren (*plus*) and this paper (*cross*). Notice that the filling factor is strongly dependent on the density of material observed.

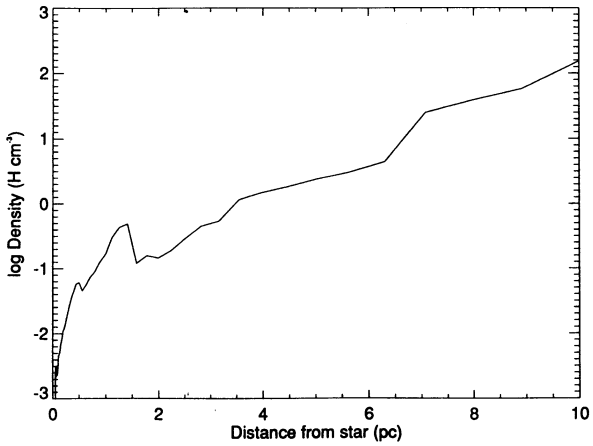

FIG. 10.—A plot of the upper limit of the gas density as a function of distance from the star. Notice the sharp drop in gas density as one approaches the star indicating that the stars must clear their immediate neighborhood of gas and dust.

gas density found by Bohlin et al. and the sharp drop in gas density as one approaches the star is a strong indication that the space near our program stars is a special environment which has been cleared of gas and dust by the star itself. Therefore the filling factors quoted in this work may not be comparable to the filling factors of the general interstellar medium.

5. COMPARISON WITH GAUSTAD & VAN BUREN

The filling factor for Gaustad & Van Buren is 0.142 ± 0.024 for dust of density greater than 0.5 H cm^{-3} and our value for the same density range is 0.05 ± 0.02. The difference is probably not a result of the inclusion of regions where there are known dust clouds, since Gaustad & Van Buren's estimate of the filling factor where their sample overlaps the sample used in this work is 0.154. The primary cause for the discrepancy is the different interpretations used. The interpretation of Gaustad & Van Buren is that the clouds are radiation-bounded; that is, the apparent size of the clouds is determined by the radiation field and clouds overlap their illuminating star, appropriate for their requirement that the clouds be centered on the star. We note that the completeness is a function of the criteria used in the survey. Because we probe a volume extending much farther from the stars than Gaustad & Van Buren, our completeness limit is much higher than theirs (their completeness limit is 0.5 H cm^{-3}), and we have seen in Figure 9 that the limit on filling factor is rising rapidly with decreasing density.

The interpretation of this paper is that at least some of the clouds are density-bounded since many of our clouds are not centered on the star. Those clouds which do not overlap the star tend to have higher densities, since low-density clouds at the same location would not be seen. Since we include clouds that are not centered on the star, we are not complete to as low a density as Gaustad & Van Buren, and this is why our filling factors are lower. Since the filling factor is so dependent on density, the best gauge of the filling factor is provided by the plot in Figure 9 which shows the filling factor of Gaustad & Van Buren as a plus sign and our value as a cross with the uncertainties on both. Both points lie above the upper limit of "all stars," but this is due mainly to the lack of dust near the O stars which dominate the total volume. Both points are consistent with the upper limit that is provided by B stars alone. Gaustad & Van Buren have assumed that the filling factor is given simply by the fraction of stars with nearby dust. If we use the same assumptions, we get a filling factor of 0.15 similar to theirs. However, this is clearly an overestimate as it assumes that all the space around each positive detection is filled with dust. If we use our model to estimate the amount of space occupied by the dust, we get a filling factor of 0.05.

6. CONCLUSION

The new survey found 194 clouds around 138 stars. We saw no evidence for a trough or hole but this may be a result of excluding the Galactic plane. Our data were reproduced well by a model with a filling factor of 0.085 for dust of density greater than 0.01 H cm^{-3}, a power-law index for cloud sizes of -4.26, a power-law index for cloud densities of -1.15, and a scale height of 250 pc. The steep index for cloud sizes implies a large amount of small-scale structure that is unresolved by *IRAS*. Our data were complete only to a density of 3.0 H cm^{-3} and the filling factor for gas above this density is 0.02 ± 0.01, consistent with our model.

Our interpretation differs from that of Gaustad & Van Buren, mainly in the assumption of whether the clouds are radiation-bounded or density-bounded. Gaustad & Van Buren assume that all of their clouds are radiation-bounded, consistent with their criterion that their clouds be centered on the star. While many of our clouds are radiation-bounded, especially in the region of late-type B stars, those near the early-type B stars and O stars are clearly not since many of those clouds are offset from the star.

REFERENCES

Bohlin, R. C., Savage, B. D., & Drake, J. F. 1978, ApJ, 224, 132
Cardelli, J. A., Clayton, G. C., & Mathis, J. S. 1989, ApJ, 345, 245
Draine, B. T., & Lee, H. M. 1984, ApJ, 285, 89
Frisch, P. C., & York, D. G. 1983, ApJ, 271, L59
Gaustad, J. E., & Van Buren, D. 1993, PASP, 105, 1127
Hoffleit, D. 1982, The Bright Star Catalog (4th Rev. Ed.) (New Haven: Yale Univ. Obs.)
Knude, J. 1979, A&AS, 38, 407
———. 1981, A&A, 98, 74
Kurucz, R. 1979, ApJS, 40, 1
Low, F. J., et al. 1984, ApJ, 278, L19
McKee, C. F., & Ostriker, J. P. 1977, ApJ, 383, 198
Murthy, J., Walker, H. J., & Henry, R. C. 1992, ApJ, 401, 574
Nandy, K., Thompson, G. I., Carnochan, D. J., & Wilson, R. 1978, MNRAS, 184, 733
Sanders, D. B., Scoville, N. Z., & Solomon, P. M. 1985, ApJ, 289, 373
Scalo, J. 1990, in Physical Processes in Fragmentation and Star Formation, (Dordrecht: Kluwer) 151
Stothers, R., & Frogel, J. A. 1974, AJ, 79, 456
Van Buren, D. 1989, ApJ, 338, 147
Zombeck, M. V. 1982, Handbook of Space Astronomy and Astrophysics (Cambridge: Cambridge Univ. Press)